Corbatón Báguena, MJ.; Vincent Vela, MC.; Alvarez Blanco, S.; Lora García, J. (2013). Analysis of Two Ultrafiltration Fouling Models and Estimation of Model Parameters as a Function of Operational Conditions. Transport in Porous Media. 99(2):391-411. doi:10.1007/s11242-013-0192-4.

Analysis of two ultrafiltration fouling models and estimation of model parameters as a function of operational conditions

María-José Corbatón-Báguena*, María-Cinta Vincent-Vela, Silvia Álvarez-Blanco, Jaime Lora-García

Department of Chemical and Nuclear Engineering, Universidad Politécnica de Valencia, C/Camino de Vera s/n 46022 Valencia, Spain

*Corresponding author: macorba@posgrado.upv.es
Tel: +34963877000 (Ext.: 76383)
Fax: +34963877639 (Ext.: 77639)

Abstract

This work analyses the measure of fit of experimental data of permeate flux decline with time for ultrafiltration experiments performed with polyethylene glycol aqueous solutions to two different ultrafiltration models. A feed solution of 5 kg/m^3 of polyethylene glycol and a monotubular ceramic membrane of ZrO_2–TiO_2 were used in the experiments. The first model considered was developed by Ho and Zydney and it considers two different fouling mechanisms: pore blocking and gel layer formation. The second model was proposed by Yee *et al.* It is an exponential model that considers three stages: concentration polarization, molecule deposition on the membrane surface and long term fouling. The results show that both models give very accurate predictions for the severe fouling conditions (high transmembrane pressures and low crossflow velocities). However, both models cannot explain the experimental results obtained for all the experimental conditions tested. An equation for Ho and Zydney's model parameters as a function of operating conditions was obtained by means of multiple regression analysis.

Keywords: Fouling dynamics; ultrafiltration; flux decline; multiple regression analysis; model parameters.

1. Introduction

Ultrafiltration (UF) is a pressure-driven separation process widely used when concentrating, purifying or separating macromolecules, colloids, and suspended particles from solutions and suspensions in many industrial fields (Wang and Song, 1999), such as water treatment, chemicals processing, food processing and biotechnology (Chan and Chen, 2004). This kind of separation-concentration process has been growing up in importance in the last decades because of its properties, such as no phase change, no chemical addition, and simple operation. Consequently, membrane processes are preferred to traditional separation methods.

Flux decline is a major problem in UF (Purkait *et al.*, 2004). The typical variation of permeate flux with time consists of an initial rapid flux decline followed by a long and gradual flux decline (Field *et al.*, 1995). The initial rapid flux decline occurs when membrane pores are blocked, whereas the long gradual flux decline is due to the accumulation of the retained particles over the membrane surface. This phenomenon, called membrane fouling, is responsible for UF membranes needing to be cleaned to restore membrane initial permeability. For that reason, mathematical modelling of the evolution of permeate flux with time is a very important tool to successfully design and operate UF plants, predicting membrane fouling and selecting the optimal operational conditions to prevent the lost of membrane properties related with fouling (Vincent-Vela *et al.*, 2010).

Membrane structure has an important influence on permeate flux improvement (de Barros *et al.*, 2003). Three situations can occur: (a) if solute molecules are smaller than the membrane pores and they enter them, irreversible fouling may appear; (b) if solute molecules and the membrane pores have a similar size, some pores can be blocked; and (c) if solute molecules are larger than the membrane pores and they are retained by the membrane, a fouling layer is formed over the membrane surface, in some cases with a gel layer structure.

Because of the non-steady state nature of UF processes, unsteady-state models are suitable to describe them (Vincent Vela *et al.*, 2008b). Empirical and theoretical models that describe ultrafiltration permeate flux decline with time can be found

in the literature and the most well-known mathematical models used in the description of membrane fouling phenomena are shown in Table 1. Empirical models are very accurate. Because of this, they are the basis of some studies (Bhattacharjee and Datta, 2003). However, they cannot explain the fouling mechanisms involved in membrane filtration. On the other hand, though theoretical models can help to understand the fouling phenomena, they are not very precise in their predictions if experimental data is not used to estimate some of their parameters. In this way, some authors (Vincent Vela *et al.*, 2009) report that the most suitable solution is to use semi-empirical models whose parameters have a physical meaning, in order to explain fouling mechanisms and to predict permeate flux decline simultaneously.

Among the different theoretical models found in the literature, the model developed by Ho and Zydney (2000) is one of the most used to fit the experimental data of UF processes due to its accurate predictions. In this way, Muthukumaran *et al.* (2005) used this model to explain the flux decay curves obtained in the UF of dairy whey solutions. The best fitting of the model was obtained at a crossflow velocity of 0.18 m/s and transmembrane pressures ranging from 0.05 to 0.3 MPa. Peng and Tremblay (2008) used Ho and Zydney's model to fit the permeate flux obtained in the MF of oily wastewaters. The best results were obtained for the tests performed at a crossflow velocity of 5-6 m/s and a transmembrane pressure of 0.2 bar. Karasu *et al.* (2010) applied Ho and Zydney's model for short time scales in the UF of a whey protein concentrate suspension at three different transmembrane pressures (0.18, 0.2 and 0.22 MPa) and three different crossflow velocities ($3 \cdot 10^{-4}$, $4.8 \cdot 10^{-4}$ and $6 \cdot 10^{-4}$ m/s). The model agreed well with experimental data for the entire UF process.

On the other hand, some authors developed semiempirical and empirical models whose equations are more simple than the ones that correspond to theoretical models. They achieved a high accuracy in the predictions. Most of these models are based on exponential equations that describe permeate flux decline with time. Mondor *et al.* (2000) used an exponential model to study the microfiltration of apple juice at a crossflow velocity of 3.3 m/s and a transmembrane pressure of 0.4 MPa. Model predictions were very accurate. Lin *et al.* (2008) used an exponential

model with four independent parameters to fit the entire flux decline flux curve obtained in the UF of aqueous solutions of BSA and hemoglobin. They divided the permeate flux decline according with two fouling phenomena: intermediate blocking for the first minutes of UF and gel layer or cake layer fouling for the rest of the UF curve. Measures of model fitting were very accurate for a transmembrane pressure of 0.35 MPa, achieving values of R^2 higher than 0.98. One of the most recent exponential models is that proposed by Yee *et al.* (2009). These authors studied the crossflow UF of whey and they also fitted Ho and Zydney's model to the experimental data obtained in the fouling experiments. Model fittings were accurate for a transmembrane pressure of 0.35 MPa, crossflow velocities ranging from 3 to 4 m/s, and a total solids concentration in fresh whey feed of 6 % (w/w), for the first 2.70 h of operation.

These authors qualitatively studied how the values of the fitted parameters of the model were influenced by the variation of some operating conditions in UF such as crossflow velocity, transmembrane pressure or feed concentration. They highlighted the importance of obtaining an equation to explain the effect of operating conditions on model parameters. Although several studies about the influence of operating conditions on membrane performance are found in the literature (Alventosa-deLara *et al.*, 2012), only few papers (Purkait *et al.*, 2004; Santafé-Moros and Gozálvez-Zafrilla, 2010) include a mathematical expression to calculate model parameters as a function of operating conditions.

In this work, the effects of transmembrane pressure and crossflow velocity on the crossflow UF of polyethylene glycol (PEG) aqueous solutions were studied. PEG has been very often used as a standard macromolecule in UF experiments to test proposed flux decline models. Bhattacharjee and Datta (2003) studied the UF of PEG-6000 aqueous solutions at a transmembrane pressure of 0.8 MPa. They developed a mathematical model that combined a resistance-in-series model with a gel polarization/film theory model. This model can predict the polarized layer resistance and the permeate flux at any time provided constant operating conditions. All the results showed a good fit for the proposed model to experimental data. Fernández-Sempere *et al.* (2009) proposed an empirical model based on the convection-diffusion mechanism and the osmotic pressure theory to

study the dead-end UF of PEG-10000 at a transmembrane pressure of 0.1 MPa. The experiments showed the existance of a reversible adsorption layer on the membrane surface. The model proposed was in good agreement with the experimental permeate flux obtained. Vincent-Vela *et al.* (2009) fitted Hermia's models adapted to crossflow UF. They used PEG aqueous solution as feed and they tested different transmembrane pressures and crossflow velocities to select the most appropriate model for operating conditions. The results showed that intermediate pore blocking is the mechanism controlling fouling at severe fouling conditions (high transmembrane pressure and low crossflow velocity). Model fitting was measured in terms of the regression coefficient R^2, achieving values up to 0.997 for severe fouling conditions.

In this paper, Ho and Zydney's model (Ho and Zydney, 2000) and the model proposed by Yee *et al.* (2009) were fitted to UF experimental data. The fitted values of model parameters were discussed in terms of their physical meaning for the different experimental conditions tested. An equation to estimate model parameters as a function of operating conditions was proposed. The use of this function allowed the estimation of model parameters without carrying out additional experimental tests or inaccurate theoretical calculations.

2. Modelling

2.1. Ho and Zydney's model

Ho and Zydney (2000) developed a model that considers two fouling mechanisms: pore blockage and gel layer formation. This mathematical model is able to explain the permeate flux values obtained over the entire filtration process, taking into account the transition between the first regime (pore blockage) and the second regime (cake formation). Thus, the model eliminates the need of different mathematical formulations to explain these two phenomena.

Permeate flux through the membrane (J) can be expressed as the sum of the flux through the open pores, J_{open}, and the flux through the partially blocked pores, $J_{blocked}$:

$$J = J_{open} + J_{blocked} \quad (1)$$

The volumetric permeate flow rates and the membrane areas for both open and covered pores are expressed as follows (Eqs. 2 to 5):

$$Q_{open} = \frac{\Delta P}{\mu R_m} A_{open} \quad (2)$$

$$A_{open} = A_m \exp\left(-\frac{\alpha \Delta P C_b}{\mu R_m} t \right) \quad (3)$$

$$Q_{blocked} = \int_{A_{blocked}} \frac{\Delta P}{\mu\left(R_m + R_p\right)} dA \quad (4)$$

$$dA_{blocked} = -dA_{open} = A_m \frac{\alpha \Delta P C_b}{\mu R_m} \exp\left(-\frac{\alpha \Delta P C_b}{\mu R_m} t \right) dt \quad (5)$$

where Q_{open} is the volumetric permeate flow rate through the open pores, ΔP is the transmembrane pressure, μ is the feed solution viscosity, R_m is the resistance of the clean membrane, A_{open} is the region of membrane area with open pores, A_m is the total membrane area, C_b is the bulk concentration, α is the pore blockage parameter, R_p is the resistance of the solute deposit, $Q_{blocked}$ is the volumetric permeate flow rate through the covered or blocked pores, $A_{blocked}$ is the region of membrane area with blocked pores and t is time.

Substituting Eq. 3 into Eq. 2 and Eq. 5 into Eq. 4, the permeate fluxes through the open and blocked pores can be determined (Eqs. 6 and 7):

$$J_{open} = J_0 \exp\left(-\frac{\alpha \Delta P C_b}{\mu R_m} t\right) \quad (6)$$

$$J_{blocked} = J_0 \int_0^t \frac{\alpha \Delta P C_b}{\mu\left(R_m + R_p\right)} \exp\left(-\frac{\alpha \Delta P C_b}{\mu R_m} t\right) dt \quad (7)$$

where J_0 is the initial permeate flux.

General equation of permeate flux as a function of time is expressed as follows (Eq. 8) by replacing Eqs. 6 and 7 into Eq. 1:

$$J = J_0 \left[\exp\left(-\frac{\alpha \Delta P C_b}{\mu R_m} t\right) + \int_0^t \frac{\alpha \Delta P C_b}{\mu\left(R_m + R_p\right)} \exp\left(-\frac{\alpha \Delta P C_b}{\mu R_m} t\right) dt \right] \quad (8)$$

Eq. 8 takes into account the temporal variation in the solute deposit resistance on the membrane surface. This is due to the fact that the solute deposit grows on the membrane surface when that region of the membrane is previously blocked by a solute aggregate. However, Ho and Zydney (Ho and Zydney, 2000) provided a general model equation much simpler (Eq. 9). They assumed a time constant resistance of the solute deposit on the membrane surface constant with time.

$$J = J_0 \left[\exp\left(-\frac{\alpha \Delta P C_b}{\mu R_m} t\right) + \frac{R_m}{R_m + R_p} \left(1 - \exp\left(-\frac{\alpha \Delta P C_b}{\mu R_m} t\right)\right) \right] \quad (9)$$

At short times, permeate flux decline is controlled by the first term. This term corresponds to the flux through the open pores and it takes into account the pore blockage mechanism. It consists of a simple exponential permeate flux decay. At long time scales, the second term dominates the filtration rate. This second term considers gel layer formation and the permeate flux through the partially blocked pores.

The two parameters involved in this model are R_p and α. The resistance of the solute deposit is expressed as follows:

$$R_p = \left(R_m + R_{p0}\right)\sqrt{1 + \frac{2f'R'\Delta PC_b}{\mu\left(R_m + R_{p0}\right)^2}t} - R_m \qquad (10)$$

where R_{p0} is the resistance of a single solute aggregate, f' is the fractional amount of total solute that contributes to the deposit growth and R' is the specific layer resistance.

The parameter α is related to the fractional amount of the total solute present as aggregate by means of Eq. (11).

$$\alpha = \frac{fA_{agg}}{M_{agg}} \qquad (11)$$

where f is the fractional amount of total solute present as aggregate, A_{agg} is the membrane area blocked by a single aggregate and M_{agg} is the mass of a single aggregate.

The model was developed assuming the following hypothesis: (a) partial pore blockage; (b) the formation of a gel layer may only occur in membrane regions with blocked pores; (c) the rate of pore coverage is proportional to the convective flow rate of molecules to the membrane surface; and (d) the permeate flux through open pores decreases exponentially with time at a rate that is proportional to the feed concentration.

Another important assumption is that the resistance of the solute deposit over the fouled surface of the membrane (R_p) is constant with time. As Ho and Zydney (2000) explained in their model development, the solute deposit grows on a certain membrane area that was previously covered or blocked by a solute aggregate. Thus, the value of R_p of those membrane regions that were blocked more recently may be lower and, therefore, have a higher permeate flux.

Considering that the value R_p is not constant over the entire filtration time, the resistance of the solute deposit will vary from its maximum value given by Eq. 10 to a value of R_{p0} in the membrane region that has just been blocked by a solute aggregate. However, the final general model equation provided by Ho and Zydney (Eq. 9) considers that R_p is constant with time.

This model was successfully applied in crossflow UF of whey and macromolecules (Muthukumaran *et al.*, 2005; Yee *et al.*, 2009; Vincent Vela *et al.*, 2007a).

2.2. Yee's model

Yee *et al.* (2009) developed a unified model to explain the permeate flux decline with time when a long-term UF process is performed. This mathematical model is able to explain permeate flux decline due to three stages: concentration polarization, molecule deposition and long-term fouling. Concentration polarization dominates the exponential permeate flux decline for the first 5-6 min of operation and it occurs due to the accumulation of foulant molecules in the vicinity of the membrane surface. After this stage flux decline is due to the deposition of molecules on the membrane surface (until the first 2-3 h). After this 3 h of operation a long-term fouling stage occurs, and the internal structure of the deposit layer formed previously may change. The reason for that is the package of the particles on the membrane surface: firstly, these molecules form a loose deposit (or glass-phase) and then, they are rearranged more orderly, forming a solid-phase. These actions result in a consolidation of the fouling layer (Yee *et al.*, 2009). When the layer on the membrane surface is consolidated, permeate flux is maintained practically constant. Therefore, the fitting lines for Yee's model become horizontal when the process reaches the steady-state condition.

The general permeate flux equation (Eq. 12) is expressed as follows:

$$J = J_\infty + k_f \exp(b_f t) \qquad (12)$$

where J_∞ is the steady-state permeate flux at the end of each fouling stage, k_f is an exponential factor that considers fouling severity and b_f is a rate constant related to the decrease in permeate flux.

Several authors (Baldasso *et al.*, 2011; Espina *et al.*, 2010; Popović *et al.*, 2009) used Yee's model to describe permeate flux decline in UF processes. Moreover, there are several studies that fitted experimental data from UF tests to an exponential model. Lin *et al.* (2008) applied the same exponential model proposed by Yee *et al.* (2009) to the dead-end UF of binary protein solutions. They divided the permeate flux decline curve in three periods. Rinaldoni *et al.* (2009) considered the entire permeate flux decline curve as one stage. They fitted an exponential model to the experimental data of the UF of skim milk for a transmembrane pressure of 0.1 MPa.

Yee *et al.* (2009) applied this model in the crossflow UF of whey and they compared the fitting of their model with the fitting of Ho and Zydney's model (Ho and Zydney, 2000).

3. Materials and methods

3.1. Materials

The PEG used to prepare the feed aqueous solution was supplied by Merck-Schuchardt (Germany). Its molecular weight distribution ranged from 28 to 38 kg/mol and its average molecular weight was 35.09167 kg/mol. To clean the membrane, aqueous solutions were prepared by dissolving NaOH pellets in deionized water. The NaOH was supplied by Panreac (Spain).

3.2. Membranes

A monotubular ceramic membrane was used for the experiments. Carbosep M2 membrane, supplied by Orelis, S.A. (France), consisted of a single cylindrical tube of 20 cm, with an external diameter of 1 cm and an internal diameter of 0.6 cm. The active layer of the membrane consisted of a ZrO_2-TiO_2 layer deposited on

the internal side of a carbon support. The membrane effective area was 35.5 cm^2, and its molecular weight cut off was 15 kg/mol.

3.3. Experimental rig

The UF pilot plant where the experiments were carried out was equipped with: pre-filters that avoid large particles to enter the pump; a variable speed pump, that allows transmembrane pressures and crossflow velocities to be modified; and a temperature control system to keep the operating temperature constant. The UF pilot plant is described elsewhere (Vincent Vela *et al.*, 2007a, Vincent Vela *et al.*, 2007b).

3.4. Experimental procedure

The experimental procedure is shown in Fig. 1. The experiments were performed as it is described in detail in Vincent Vela *et al.* (2008a), Vincent Vela *et al.* (2008b) and Vincent Vela *et al.* (2009). A complete fouling-cleaning experiment consisted of four steps (fouling, rinsing, cleaning and rinsing). They were carried out at the operating conditions of concentration, temperature, transmembrane pressure (ΔP) and crossflow velocity (v) shown in Fig. 1. After each complete experimental run, it was checked that the initial membrane permeability was completely restored.

3.5. FESEM membrane characterization

The membrane used in the experiments was analysed with a field emission scanning electron microscope (FESEM). The fouling experiment was carried out at the most severe fouling conditions tested (a transmembrane pressure of 0.4 MPa and a crossflow velocity of 1 m/s).

4. Results and discussion

The value of the membrane resistance obtained in the experiments performed with deionised water was $6.897 \cdot 10^{12}$ m^{-1}.

The experimental data that corresponds to the fouling UF tests were smoothed using the MathCad® supsmooth tool. This tool uses linear least squares fitting to minimize the experimental error that may occur in the original data. The fitting of the models to the experimental data was carried out using the MathCad® Genfit algorithm. The Genfit algorithm employs an optimized version of the Levenberg-Marquadt method for the minimization of the overall difference between experimental results and the predicted ones, for each experimental condition tested.

4.1. Membrane cross-section analysis by FESEM

Fig. 2 shows the FESEM images for the new membrane (a) and the membrane fouled with PEG (b). As it can be observed, membrane surface in Fig. 2a is smoother than the membrane surface in Fig. 2b. In addition, the original roughness of the membrane can be observed in Fig. 2a, whereas a fouling layer deposited over the active layer of the membrane is shown in Fig. 2b. This is due to the fact that PEG mainly deposited on the membrane surface at long operation times (7 hours). PEG formed a cake layer on the membrane surface. This is in agreement with the Ho and Zydney's model studied in this work (Ho and Zydney, 2000), which considers that cake formation is the fouling mechanism responsible for the long term fouling.

4.2. Ho and Zydney's model fitting

Figs. 3 to 5 show the fitting of Ho and Zydney's model (solid lines) to the experimental results, according to Eq. (9). The experimental results (Figs. 3-5) confirm that the combination of high transmembrane pressures and low crossflow velocities favour the accumulation of solute molecules on the membrane surface (Vincent Vela *et al.*, 2009). For short time scales and a constant crossflow velocity, the rate of the initial permeate flux decline increases as transmembrane pressure increases (Fig. 3). This is in agreement with Ho and Zydney's model. This model considers that the initial permeate flux decline is due to the pore blocking phenomenon and that pore blocking is more severe as transmembrane

377 pressure increases (Mondal and De, 2010). When the crossflow velocity decreases
378 and the transmembrane pressure is kept constant, permeate flux decline at short
379 time scales increases (Figs. 3-5). However, the rate of initial permeate flux decline
380 increases faster when transmembrane pressure increases than in the case of
381 increasing crossflow velocity. This confirms that pore blocking is more likely to
382 occur when transmembrane pressure increases rather than in the case of
383 decreasing crossflow velocity. It must be noticed that although the molecular
384 weight of the PEG used in the fouling tests was higher (35 kg/mol) than the
385 MWCO of the membrane (15 kg/mol), pore blocking was occurring for low time
386 scales during the experiments. This occurs because PEG is a polymeric
387 macromolecule which has a linear and flexible structure (Bhattacharjee and Datta,
388 2003). Thus, PEG molecules may be oriented in the direction of the membrane
389 pores and may enter them. For high crossflow velocities and low transmembrane
390 pressures, no pore blocking phenomenon may occur under the experimental
391 conditions tested as the permeate flux does not decrease exponentially with time
392 (Fig. 5). Therefore, pore blocking is more likely to occur at severe fouling
393 conditions (see Fig. 3).
394
395 Figs. 3 to 5 also show that the long-term permeate flux is stable with time. This
396 behaviour supports the theory explained in (Buetehorn *et al.*, 2010), which is
397 based on the equilibrium between the retention of solute molecules and the back-
398 transport of deposited particles due to the convective flow. When this equilibrium
399 is achieved, a constant permeate flux is obtained. Ho and Zydney's model
400 predictions as well as experimental results show that, at low crossflow velocities,
401 the steady-state permeate flux is more similar for all the transmembrane pressures
402 tested (Fig. 3) than in the case of high crossflow velocities (Fig. 3 and 4). When
403 the transmembrane pressure increases, both the driving force of the filtration
404 process and the filtration resistance increase. For low crossflow velocities and
405 high transmembrane pressures, these opposed effects can compensate each other
406 and the long term permeate flux becomes independent of the transmembrane
407 pressure. On the other hand, the crossflow velocity has an important effect over
408 the long term permeate flux. For each transmembrane pressure tested, steady-state
409 permeate fluxes increase as crossflow velocity increases. This effect is more
410 noticeable for high transmembrane pressures. For example, the difference between

411 the steady-state permeate flux for a crossflow velocity of 1 m/s and 3 m/s at 0.4
412 MPa is much higher than the difference between those values at a transmembrane
413 pressure of 0.1 MPa (see Figs. 3 and 5). If the crossflow velocity increases, the
414 back-transport of deposited molecules due to convective flow may increase,
415 without having an effect over the driving force of the process. Thus, the filtration
416 resistance decreases and the permeate flux increases (Buetehorn *et al.*, 2010).
417
418 The accuracy of model predictions is expressed in terms of R^2 (Table 2). The best
419 fittings were obtained for a crossflow velocity of 1 m/s and transmembrane
420 pressures of 0.2, 0.3 and 0.4 MPa, a crossflow velocity of 2 m/s and
421 transmembrane pressures of 0.2, 0.3 and 0.4 MPa and a crossflow velocity of 3
422 m/s and transmembrane pressures of 0.3 and 0.4 MPa. For these experimental
423 conditions, that correspond to high fouling conditions, the values of R^2 ranged
424 from 0.945 to 0.995. Thus, Ho and Zydney's model fits reasonably well to
425 experimental data in the case of high transmembrane pressures and low crossflow
426 velocities (severe fouling conditions).
427
428 It is important to note that, although the values of R^2 are good for high
429 transmembrane pressure, in the case of a transmembrane pressure of 0.4 MPa and
430 a crossflow velocity of 1 m/s the experimental permeate flux decays faster than
431 the permeate flux predicted by Ho and Zydney's model (see Fig. 3) and, thus, the
432 predicted values cannot reflect accurately the slow decay at longer times.
433
434 In the previous work carried out by Vincent Vela *et al.* (2008b), the same general
435 equation of Ho and Zydney's model as the one used in our work was fitted to the
436 experimental data using theoretical estimations of the model parameters. In
437 addition, some of these theoretical estimations assume that the PEG molecule is
438 spherical. However, some authors reported that the structure of PEG is linear and
439 flexible (Bhattacharjee and Datta, 2003). However, in this work, theoretical
440 estimations of model parameters that result in low fitting accuracy were not
441 performed. Empirical estimations were used. When comparing Ho and Zydney's
442 model in both studies it can be seen that in this work (Figs. 3 to 5), the fitting
443 accuracy was higher than in previous work (Figs. 1 to 3 in Vincent Vela *et al.*
444 (2008b)).

On the other hand, Hermia's models were fitted to the experimental data presented in this manuscript in previous works of Vincent Vela *et al.* (Vincent Vela *et al.*, 2008a; Vincent Vela *et al.*, 2009). Model parameters were theoretically estimated in Vincent Vela *et al.* (2008a), whereas the same parameters were empirically estimated in Vincent Vela *et al.* (2009). Although empirical estimation of Hermia's model parameters is more accurate than theoretical estimations, due to the assumptions considered in the theoretical estimations, differences between the values of R^2 for model predictions are about 5 %. Thus, theoretical estimations of model parameters are preferred because the difference between both predictions in terms of R^2 is low and the model parameters theoretically estimated provide a better understanding of the physics of the process.

Comparing Hermia's models whose parameters were theoretically estimated (Vincent Vela *et al.*, 2008a) and the Ho and Zydney's model whose parameters were empirically estimated, it can be observed that both models provide explanations about the fouling phenomena that cause permeate flux decline with time. In both cases, model predictions were accurate for severe fouling conditions (high transmembrane pressures and low crossflow velocities). However, Hermia's models provide a more detailed description of the types of pore blocking mechanisms. However, Ho and Zydney's model only considers that pore blocking is responsible for the initial permeate flux decline. On the other hand, the general model equation developed by Ho and Zydney's combines two main mechanisms of membrane fouling (pore blocking and cake formation) in the same general equation. This allows a more simplified estimation of permeate flux decline.

4.3. Yee's model fitting

Figs. 3 to 5 also show the fitting of Yee's model to the experimental results, according to Eq. 12. When comparing Ho and Zydney's model predictions (dotted lines) with Yee's model predictions (solid lines), it can be observed that both models achieve very similar predictions.

Yee's model can also be fitted to experimental data considering three fouling stages (Yee *et al.*, 2009). To select the time at which membrane fouling changed from one stage to another Eq. 12 was linearized (Eq. 13):

$$\ln(J\text{-}J_\infty) = \ln(k_f) + b_f\, t \qquad (13)$$

Fig. 6 shows the experimental results for PEG UF expressed as $\ln(J\text{-}J_\infty)$ as a function of time for a transmembrane pressure of 0.4 MPa and a crossflow velocity of 1 m/s. As it can be observed the results follow three linear equations with three different slopes that correspond to the three stages previously mentioned. For each fouling stage, the parameters of the model (k_f and b_f) were fitted to the experimental data. The results are shown in Table 3, when three stages were considered and in Table 4 when only one stage was taken into account.

Yee's model fitting accuracy for each experimental condition tested, expressed as R^2, is shown in Tables 5 and 6, for three stages and one stage, respectively. In both cases, the best fittings were obtained for the same experimental conditions as in Ho and Zydney's model. The values of R^2 for these experimental conditions ranged from 0.951 to 0.994, in the case of one fouling stage, and from 0.972 to 0.997, in the case of three fouling stages. Therefore, it can be concluded that both models have similar accuracy.

Although the models studied have a similar accuracy in terms of R^2 for all the experimental conditions tested, the main difference between them is that Ho and Zydney's model is a theoretical model whose parameters have physical meaning and Yee's model is an empirical model whose parameters do not have a physical meaning. In general, theoretical models are preferred to empirical ones because they provide an explanation of the physics of the process.

Yee *et al.* (2009) found that Ho and Zydney's model was able to predict permeate flux decline when the decrease in permeate flux was due to concentration polarization and solute molecule deposition mechanisms. This situation occurred at the first 3 h of operation in the whey UF experiments carried out by Yee *et al.*

512 (2009). However, for the rest of the operation time the model developed by Ho
513 and Zydney failed. In the case of the experimental data presented in this
514 manuscript, both models explained with a great accuracy the decrease in permeate
515 flux with time over the entire UF time for the experimental conditions that
516 correspond to high fouling conditions.
517

518 **4.4. Influence of the operating conditions on the model parameters**

519 Table 7 shows the fitted parameters, α and R_p, for Ho and Zydney's model for the
520 experimental conditions that correspond to high values of R^2. For those
521 experimental conditions membrane fouling is noticeable and Ho and Zydney's
522 model accuracy is high. It can be observed that R_p increases as transmembrane
523 pressure increases and it decreases as crossflow velocity increases. This is in
524 accordance with the fact that R_p represents the gel layer resistance. As it was
525 expected, R_p is higher for severe fouling conditions (high transmembrane
526 pressures and low crossflow velocities). Furthermore, for high fouling conditions,
527 an increase in transmembrane pressure or a decrease in crossflow velocity has
528 more influence on the values of R_p than in the case of low fouling conditions. For
529 severe fouling conditions the blocked membrane area, α, increases as
530 transmembrane pressure increases. Comparing the values of α at a crossflow
531 velocity of 1 m/s and transmembrane pressures of 0.3 and 0.4 MPa (5.898 and
532 6.782, respectively), it can be observed that an increase in transmembrane
533 pressure results in an increase in the value of the parameter (see Table 7).
534 However, the pattern of α with the crossflow velocity is not clear.
535
536 The fitted model parameters of Ho and Zydney's model (Table 7) were correlated
537 with transmembrane pressure and crossflow velocity by means of a multiple
538 regression using Statgraphics®. The first regression analysis was performed
539 considering double interactions for transmembrane pressure and crossflow
540 velocity: ΔP, v, ΔP^2, v^2, and $v \cdot \Delta P$. The coefficients of the regression model that
541 showed the greatest p-values were dropped and a new regression analysis was
542 performed. All model parameters were expressed as a function of transmembrane
543 pressure, crossflow velocity and their interactions (Eqs. (14) and (15)). To obtain

these equations, several multiple regression analysis (MRA) were performed (Table 8), taking into account the following operating conditions:

- MRA 1: 1 m/s and 0.2, 0.3 and 0.4 MPa; 2 m/s and 0.3 and 0.4 MPa; 3 m/s and 0.3 and 0.4 MPa.
- MRA 2: 1 m/s and 0.3 and 0.4 MPa; 2 m/s and 0.3 and 0.4 MPa; 3 m/s and 0.3 and 0.4 MPa.
- MRA 3: 1 m/s and 0.3 and 0.4 MPa; 2 m/s and 0.3 and 0.4 MPa; 3 m/s and 0.4 MPa.
- MRA 4: 1 m/s and 0.3 and 0.4 MPa; 2 m/s and 0.3 and 0.4 MPa.

The use of several MRA that corresponded to high fouling conditions allowed to obtain the equation for R_p and α as a function of transmembrane pressure and crossflow velocity that presented the highest value of R^2. According to Eq. 10, R_p is a function of transmembrane pressure and the specific layer resistance, R', which also depends on the crossflow velocity. Some authors also related α and R_p to transmembrane pressure and crossflow velocity (Muthukumaran *et al.*, 2005; Karasu *et al.*, 2010). In addition, both parameters can be considered constant with time, according to the above mentioned references and the assumptions of the Ho and Zydney's work (Ho and Zydney, 2000). However, although the model parameters of Ho and Zydney's model can be related to the operating conditions by means of Eqs. 14 and 15, these functional relations may not capture the physics of the process.

Table 8 shows the values of the linear regression coefficient R^2 for the MRA performed. The highest value of R^2 for R_p was obtained with MRA 2 (R^2 = 0.965). Therefore, MRA 2 was selected as the best multiple regression analysis for the parameter R_p. Regarding to the parameter α, the multiple regression analysis with the highest R^2 (0.884) was MRA 4. The final model equations obtained for R_p and α according with the best MRAs were Eqs. (14) and (15), respectively.

$$R_p = -2.49480 \cdot 10^{13} + 1.35698 \cdot 10^{8} \cdot \Delta P + 3.14208 \cdot 10^{12} \cdot v^2 - 4.69607 \cdot 10^{7} \cdot v \cdot \Delta P \quad (14)$$

$$\alpha = 9.54497 - 9.54898 \cdot 10^{-6} \cdot \Delta P \cdot v \quad (15)$$

Table 4 shows the fitted parameters, k_f and b_f, for Yee's model when one fouling stage is considered for the experimental conditions that correspond to high values of R^2. According to Yee's model, the parameter k_f is related with how fast is the exponential decrease in permeate flux at short time scales. In this way, when transmembrane pressure increases and crossflow velocity decreases, the exponential decrease in permeate flux is faster and the parameter k_f increases (Table 4). Therefore, k_f is higher for severe fouling conditions (high transmembrane pressures and low crossflow velocities). Table 4 also shows that b_f follows the same pattern as k_f with transmembrane pressure and crossflow velocity, for severe fouling conditions. The values of b_f are related to how foulant molecules accumulate on the membrane surface and to the fundamental structure of the gel layer when particle deposition is the dominant fouling mechanism. When transmembrane pressure increases, convection of the solute molecules towards the membrane surface is enhanced and the accumulation of these molecules near the membrane surface is promoted. Thus, the time required to develop the boundary layer is reduced. It must be noticed that b_f (Table 4) follows the same pattern as R_p (Table 7) with transmembrane pressure and crossflow velocity. This behaviour was expected since b_f and R_p are both related to the same fouling mechanism (gel layer formation) (Yee *et al.*, 2009).

Tables 3 and 9 show the fitted parameters and the transition time, respectively, for Yee's model when three stages are considered. The transition time t_1 between the stage 1 (dominated by concentration polarization) and the stage 2 (controlled by molecules deposition) decreases when transmembrane pressure increases in the case of severe fouling conditions. This is due to the fact that high transmembrane pressures favour molecules deposition on the membrane surface and stage 2 occurs at lower times.

Table 3 shows the values of the fitted parameters k_f and b_f for Yee's model when three stages are considered. The parameter k_f follows the same pattern with transmembrane pressure and crossflow velocity when one (Table 4) and three (Table 3) stages are considered. Thus, k_f is high in the case of severe fouling conditions (high transmembrane pressures and low crossflow velocities),

independently of the number of stages considered. For stage 1, the parameter b_f (Table 3) follows the same pattern with transmembrane pressure and crossflow velocity as k_f (Table 3) and b_f (Table 4). However, this behaviour is not observed for b_f at stages 2 and 3 (Table 3). This is due to the fact that, once the molecule deposition occurred, an increase in transmembrane pressure did not result in a higher permeate flux decrease, because the convection of solute molecules towards the membrane surface is balanced with the back diffusion to the bulk solution (Yee *et al.*, 2009).

On the other hand, in the case of the Yee's model for one stage and three stages, it was not possible to establish correlations between the fitted parameters and the operating conditions because the values of R^2 obtained were very low.

When substituting the equations that related the model parameters of Ho and Zydney's model with the operating conditions (Eqs. 14 and 15) into the general model equation (Eq. 9), a modified model was obtained. However, due to the low accuracy in the estimation of the parameter α (R^2=0.884), only the equation of the parameter R_p (Eq. 14) was substituted in Eq. 9 and the value obtained for α in Table 7 was used instead of Eq. 15. The results show that similar accuracy in terms of R^2 was obtained for the highest transmembrane pressure studied (0.4 MPa) and all the crossflow velocities tested for the original model of Ho and Zydney (Table 2) and the modified one (0.985, 0.899 and 0.989 for a transmembrane pressure of 0.4 MPa and crossflow velocities of 1, 2 and 3 m/s, respectively). However, the accuracy of the modified model is much lower than the original Ho and Zydney's one in terms of R^2 at lower transmembrane pressures.

5. Conclusions

The innovation of the current work is the development of Eqs. 14 and 15 that allow the determination of Ho and Zydney model parameters as a function of operating conditions without performing experimental tests or inaccurate theoretical calculations. Another important innovation is that the model developed by Yee *et al.* was fitted to the entire permeate flux decline curve without dividing

it in three stages. We obtained that both models (for one fouling stage and considering three stages) provided similar accuracy in terms of R^2. Yee's model with one fouling stage is preferred to Yee's model considering three stages because it simplifies model predictions.

The models studied in this work cannot explain the experimental results obtained for all the experimental conditions tested. Only in the case of high transmembrane pressures and low crossflow velocities, both models provide very accurate fitting to experimental data of permeate flux decline with time. Models studied may fail for those experimental conditions at which some model hypothesis are not valid, such as low fouling conditions (low transmembrane pressures and high crossflow velocities). To improve the accuracy of Ho and Zydney's model at those experimental conditions, one possible solution could be estimating the permeate flux without considering the resistance of the solute layer to be constant with time. Although this estimation is more complex than the analytical solution proposed by Ho and Zydney, it is expected that its predictions to be more accurate for all the experimental conditions tested. On the other hand, the analytical solution (Eq. 9) could be used dividing the entire fouling decline curve in several stages, as Yee *et al.* (2009) did with their exponential model.

In the case of Yee's model, model prediction accuracy for one and three stages was similar in terms of R^2.

An equation that relates Ho and Zydney's model parameters as a function of experimental conditions was obtained by means of multiple regression analysis. Multiple regression analysis applied to Yee's model parameters did not result in a valid equation for these parameters as a function of operating conditions.

Acknowledgements

The authors of this work wish to gratefully acknowledge the financial support of the Universidad Politécnica de Valencia through the project no. 2010.1009 and the Spanish Ministry of Science and Technology through the project CTM2010-20186.

Nomenclature

List of symbols

A	Transport area (m^2)
A_{agg}	Membrane area blocked by a single aggregate (m^2)
A_{open}	Region of membrane area with open pores (m^2)
$A_{blocked}$	Region of membrane area with partially blocked pores (m^2)
A_m	Membrane area (m^2)
B	Constant in complete blocking law (s^{-1})
b_f	Rate constant for the decrease in flux decline in each stage of fouling (s^{-1})
C	Constant in standard blocking law (s^{-1})
C_b	Bulk concentration (kg/m^3)
C_g	Gel concentration (kg/m^3)
C_p	Permeate concentration (kg/m^3)
D	Particle diffusion coefficient
f	Fractional amount of the total solute present as aggregate (dimensionless)
f‘	Fractional amount of the total solute that contributes to the deposit growth (dimensionless)
J	Permeate flux ($m^3 \cdot m^{-2} \cdot s^{-1}$)
$\overline{J}$	Average permeate flux ($m^3 \cdot m^{-2} \cdot s^{-1}$)
J_{eq}	Local equilibrium permeate flux ($m^3 \cdot m^{-2} \cdot s^{-1}$)
J_{open}	Permeate flux through the open pores ($m^3 \cdot m^{-2} \cdot s^{-1}$)
$J_{blocked}$	Permeate flux trough the partially blocked pores ($m^3 \cdot m^{-2} \cdot s^{-1}$)
J_0	Initial permeate flux ($m^3 \cdot m^{-2} \cdot s^{-1}$)
J_∞	Steady-state permeate flux ($m^3 \cdot m^{-2} \cdot s^{-1}$)
J_w	Deionized water flux ($m^3 \cdot m^{-2} \cdot s^{-1}$)
k_b	Back transport coefficient
k_f	Exponential factor for each stage of fouling ($m^3 \cdot m^{-2} \cdot s^{-1}$)
L	Membrane length (m)
M_{agg}	Mass of a single aggregate (kg)
P_m	Permeability coefficient
ΔP	Transmembrane pressure (MPa)
Q_{open}	Volumetric permeate flow rate through open pores ($m^3 \cdot s^{-1}$)
$Q_{blocked}$	Volumetric permeate flow rate through partially blocked pores ($m^3 \cdot s^{-1}$)
R_a	Resistance of the irreversible adsorbed protein deposit (m^{-1})

711 R_m Resistance of the clean membrane (m^{-1})
712 R_p Resistance of the solute deposit (m^{-1})
713 R_{p0} Resistance of a single solute aggregate (m^{-1})
714 R' Specific layer resistance (m/kg)
715 t Filtration time (s)
716 t_1 Transition time between fouling stages 1 and 2 (s)
717 t_2 Transition time between fouling stages 2 and 3 (s)
718 t_{ss} Steady state time (s)
719 V Total volume collected (m^3)
720 x Distance from the membrane entrance (m)
721
722 Greek letters
723 α Pore blockage parameter (m^2/kg)
724 β Fraction of pores susceptible to be completely blocked (dimensionless)
725 γ Shear rate
726 μ Feed solution viscosity ($kg \cdot m^{-1} \cdot s^{-1}$)
727 σ Rejection
728 ω Angular velocity ($rad \cdot s^{-1}$)
729 Δπ Osmotic pressure
730
731 Abbreviations
732 UF Ultrafiltration
733 PEG Polyethylene glycol
734 MRA Multiple regression analysis
735

736 # References

737 Alventosa-deLara E., Barredo-Damas S., Alcaina-Miranda M.I., Iborra-Clar M.I.: Ultrafiltration
738 technology with a ceramic membrane for reactive dye removal: Optimization of membrane
739 performance. J. Hazard. Mater. 209-210, 492-500 (2012).
740 Baldasso C., Barros T.C., Tessaro I.C.: Concentration and purification of whey proteins by
741 ultrafiltration. Desalination 278, 381-386 (2011).
742 Bhattacharjee C., Datta S.: Analysis of polarized layer resistance during ultrafiltration of PEG-
743 6000: an approach based on filtration theory. Sep. Purif. Technol. 33, 115-126 (2003).

744 Buetehorn S., Carstensen F., Wintgens T., Melin T., Volmering D., Vossenkaul K.: Permeate flux
745 decline in crossflow microfiltration at constant pressure. Desalination 250, 985-990 (2010).
746 Chan R., Chen V.: Characterization of protein fouling on membranes: opportunities and
747 challenges. J. Membr. Sci. 242, 169-188 (2004).
748 Cheryan M.: Ultrafiltration and Microfiltration Handbook. Technomic Publishing Company, Inc.,
749 1998.
750 de Barros S.T.D., Andrade C.M.G., Mendes E.S., Peres L.: Study of fouling mechanism in
751 pineapple juice clarification by ultrafiltration. J. Membr. Sci. 215, 213-224 (2003).
752 de la Casa E.J., Guadix A., Ibáñez R., Camacho F., Guadix E.M.: A combined fouling model to
753 describe the influence of the electrostatic environment on the cross-flow microfiltration of BSA. J.
754 Membr. Sci. 318, 247-254 (2008).
755 Espina V., Jaffrin M.Y., Ding L., Cancino B.: Fractionation of pasteurized skim milk proteins by
756 dynamic filtration. Food Res. Int. 43, 1335-1346 (2010).
757 Fernández-Sempere J., Ruiz-Beviá F., García-Algado P., Salcedo-Díaz R.: Visualization and
758 modeling of the polarization layer and a reversible adsorption process in PEG-10000 dead-end
759 ultrafiltration. J. Membr. Sci. 342, 279-290 (2009).
760 Field R.W., Wu D., Howell J.A., Gupta B.B.: Critical flux concept for microfiltration fouling. J.
761 Membr. Sci. 100, 259-272 (1995).
762 Hermia J.: Constant pressure blocking filtration laws – application to powerlaw non-newtonian
763 fluids. Trans. IChemE, 60, 183-187 (1982).
764 Ho C-C., Zydney A.L.: A combined pore blockage and cake filtration model for protein fouling
765 during microfiltration. J. Colloid Interface Sci. 232, 389-399 (2000).
766 Karasu K., Yoshikawa S., Ookawara S., Ogawa K., Kentish S.E., Stevens G.W.: A combined
767 model for the prediction of the permeation flux during the cross-flow ultrafiltration of a whey
768 suspension. J. Membr. Sci. 361, 71-77 (2010).
769 Ko M.K., Pellegrino J.J.: Determination of osmotic pressure and fouling resistances and their
770 effects on performance of ultrafiltration membranes. J. Membr. Sci. 74, 141-157 (1992).
771 Lee N., Amy G., Croué J-P., Buisson H.: Morphological analyses of natural organic matter (NOM)
772 fouling of low-pressure membranes (MF/UF). J. Membr. Sci. 261, 7-16 (2005).
773 Lin S-H., Hung C-L., Juang R-S.: Applicability of the exponential time dependence of flux decline
774 during dead-end ultrafiltration of binary protein solutions. Chem. Eng. J. 145, 211-217 (2008).
775 Mondal S., De S.: A fouling model for steady state crossflow membrane filtration considering
776 sequential intermediate pore blocking and cake formation. Sep. Purif. Technol. 75, 222-228
777 (2010).
778 Mondor M., Girard B., Moresoli C.: Modeling flux behaviour for membrane filtration of apple
779 juice. Food Res. Int. 33, 539-548 (2000).
780 Muthukumaran S., Kentish S.E., Ashokkumar M., Stevens G.W.: Mechanisms for the ultrasonic
781 enhancement of dairy whey ultrafiltration. J. Membr. Sci. 258, 106-114 (2005).
782 Peng H., Tremblay A.Y.: Membrane regeneration and filtration modeling in treating oily
783 wastewaters. J. Membr. Sci. 324, 59-66 (2008).

784 Popović S., Milanović S., Iličić M., Djurić M., Tekić M.: Flux recovery of tubular ceramic
785 membranes fouled with whey proteins. Desalination 249, 293-300 (2009).
786 Purkait M.K., DasGupta S., De S.: Resistance in series model for micellar enhanced ultrafiltration
787 of eosin dye. J. Colloid Interface Sci. 270, 496-506 (2004).
788 Rinaldoni A.N., Taragaza C.C., Campderrós M.E., Pérez Padilla A.: Assessing performance of
789 skim milk ultrafiltration by using technical parameters. J. Food Eng. 92, 226-232 (2009).
790 Santafé-Moros A., Gozálvez-Zafrilla J.M.: Nanofiltration study of the interaction between
791 bicarbonate and nitrate ions. Desalination 250, 773-777 (2010).
792 Song L.: Flux decline in crossflow microfiltration and ultrafiltration: mechanisms and modeling of
793 membrane fouling. J. Membr. Sci. 139, 183-200 (1998).
794 Vincent Vela M.C., Álvarez Blanco S., Lora García J., Gozálvez Zafrilla J.M., Bergantiños
795 Rodríguez E.: Modelling of flux decline in crossflow ultrafiltration of macromolecules:
796 comparison between predicted and experimental results. Desalination 204, 328-334 (2007a).
797 Vincent Vela M.C., Álvarez Blanco S., Lora García J., Gozálvez Zafrilla J.M., Bergantiños
798 Rodríguez E.: Utilization of a shear induced diffusion model to predict permeate flux in the
799 crossflow ultrafiltration of macromolecules. Desalination 206, 61-68 (2007b).
800 Vincent Vela M.C., Álvarez Blanco S., Lora García J., Bergantiños Rodríguez E.: Analysis of
801 membrane pore blocking models applied to the ultrafiltration of PEG. Sep. Purif. Technol. 62,
802 489-498 (2008a).
803 Vincent Vela M.C., Álvarez Blanco S., Lora García J., Bergantiños Rodríguez E.: Fouling
804 dynamics modelling in the ultrafiltration of PEGs. Desalination 222, 451-456 (2008b).
805 Vincent Vela M.C., Álvarez Blanco S., Lora García J., Bergantiños Rodríguez E.: Analysis of
806 membrane pore blocking models to crossflow ultrafiltration in the ultrafiltration of PEG. Chem.
807 Eng. J. 149, 232-241 (2009).
808 Vincent-Vela C., Cuartas-Uribe B., Álvarez-Blanco S., Lora-García J., Bergantiños-Rodríguez E.:
809 Analysis of ultrafiltration processes with dilatant macromolecular solutions by means of
810 dimensionless numbers and hydrodynamic parameters. Sep. Purif. Technol. 75, 332-339 (2010).
811 Wang L., Song L.: Flux decline in crossflow microfiltration and ultrafiltration: experimental
812 verification of fouling dynamics. J. Membr. Sci. 160, 41-50 (1999).
813 Yee K.W.K., Wiley D.E., Bao J.: A unified model of the time dependence of flux decline for the
814 long-term ultrafiltration of whey. J. Membr. Sci. 332, 69-70 (2009).
815

816 # Figure legends

817 **Fig. 1** Experimental procedure

818 **Fig. 2** Cross-section of new (a) and fouled (b) membranes at X27800 of magnification

819 **Fig. 3** Permeate flux predictions for Ho and Zydney's model (dotted line) and Yee's model for one
820 stage (solid line) at different transmembrane pressures for a crossflow velocity of 1 m/s, (symbols:
821 experimental data)

Fig. 4 Permeate flux predictions for Ho and Zydney's model (dotted line) and Yee's model for one stage (solid line) at different transmembrane pressures for a crossflow velocity of 2 m/s, (symbols: experimental data)

Fig. 5 Permeate flux predictions for Ho and Zydney's model (dotted line) and Yee's model for one stage (solid line) at different transmembrane pressures for a crossflow velocity of 3 m/s, (symbols: experimental data)

Fig. 6 Evolution of $\ln(J\text{-}J_\infty)$ with time for a transmembrane pressure of 0.4 MPa and a crossflow velocity of 1 m/s, (lines: estimated results; symbols: experimental data)

Tables

Table 1

Mathematical models used in the prediction of fouling phenomena.

General equation	Reference
$-\frac{dJ}{dt} = K(J - J_\infty)J^{2-n}$	Hermia (1982)
$J(t) = J_0 Q^{-b}$	Cheryan (1998)
$J(t) = J_\infty + k\exp(-ct)$	Lin *et al.* (2008)
$J = \beta J_0 \exp(-Bt) + (1-\beta)\frac{J_0}{(1+Ct)^2}$	De la Casa *et al.* (2008)
$J = \frac{\Delta P - \sigma\Delta\pi}{\mu(R_m + R_a + R_p)}$	Ko and Pellegrino (1992)
$\frac{1}{J} = \frac{\mu R_m}{\Delta P} + \frac{\mu}{P_m \Delta P} \times \left[\frac{V}{A}\left(\frac{C_b - C_p}{C_g - C_b}\right) - \frac{k_b}{A}\frac{C_g}{C_g - C_b}\omega t\right]$	Bhattachrajee and Datta (2003)
$\overline{J}(t) = \begin{cases} \frac{1}{L}\left[\int_0^{x(t)} J_{eq}(x)dx + [L - x(t)]J(t)\right] & \text{when } t < t_{ss} \\ 1.31\left(D^2\gamma/L\right)^{1/3}\left(C_g/C_0 - 1\right)^{1/3} & \text{when } t \geq t_{ss} \end{cases}$	Song (1998)

Table 2

Measures of fit for Ho and Zydney's model: values of R^2.

ΔP (MPa)	v (m/s)	R^2
0.1		0.538
0.2	1	0.993
0.3		0.988
0.4		0.986
0.1		0.781
0.2	2	0.945
0.3		0.995
0.4		0.980
0.1		0.954
0.2	3	0.921
0.3		0.967
0.4		0.991

Table 3

Fitted Yee's model parameters for each stage.

ΔP	v	Stage 1		Stage 2		Stage 3	
(MPa)	(m/s)	$k_f \cdot 10^7$ ($m^3/m^2 \cdot s$)	$-b_f \cdot 10^4$ (s^{-1})	$k_f \cdot 10^7$ ($m^3/m^2 \cdot s$)	$-b_f \cdot 10^4$ (s^{-1})	$k_f \cdot 10^7$ ($m^3/m^2 \cdot s$)	$-b_f \cdot 10^4$ (s^{-1})
0.2		3.10	19.92	41.12	12.90	16.98	1.82
0.3	1	16.95	34.25	62.04	9.44	41.70	1.40
0.4		97.79	51.62	247.11	6.77	150.52	1.53
0.2		10.21	9.15	52.84	4.94	294.19	6.04
0.3	2	3.55	13.40	41.33	5.26	48.83	1.30
0.4		55.80	44.48	103.23	46.90	17.66	0.71
0.2		91.91	8.42	40.68	3.98	26.95	1.56
0.3	3	20.77	56.67	45.89	4.38	33.96	1.35
0.4		11.23	30.76	50.57	2.55	228.06	2.18

Table 4

Fitted Yee's model parameters for one stage.

ΔP (MPa)	v (m/s)	$k_f \cdot 10^7$ ($m^3/m^2 \cdot s$)	$-b_f \cdot 10^4$ (s^{-1})
0.2		24.93	2.59
0.3	1	62.32	2.17
0.4		292.20	3.24
0.2		22.62	2.27
0.3	2	43.33	1.15
0.4		109.00	3.40
0.2		26.91	1.46
0.3	3	53.27	2.10
0.4		50.83	1.55

Table 5

Measures of fit for Yee's model: values of R^2 for each stage.

ΔP (MPa)	v (m/s)	R^2 Stage 1	R^2 Stage 2	R^2 Stage 3
0.1		0.922	0.990	0.970
0.2	1	0.985	0.958	0.997
0.3		0.981	0.908	0.987
0.4		0.975	0.993	0.994
0.1		0.929	0.844	0.928
0.2	2	0.973	0.984	0.972
0.3		0.996	0.942	0.993
0.4		0.949	0.992	0.944
0.1		0.945	0.965	0.960
0.2	3	0.935	0.989	0.943
0.3		0.968	0.969	0.984
0.4		0.936	0.973	0.934

884 Table 6

885 Measures of one stage fit for Yee's model: values of R^2.

ΔP (MPa)	v (m/s)	R^2
0.1		0.842
0.2	1	0.992
0.3		0.983
0.4		0.982
0.1		0.886
0.2	2	0.951
0.3		0.994
0.4		0.980
0.1		0.964
0.2	3	0.968
0.3		0.981
0.4		0.993

886

887 Table 7

888 Fitted Ho and Zydney's model parameters.

ΔP (MPa)	v (m/s)	α (m^2/kg)	$R_p \cdot 10^{-13}$ (m^{-1})
0.2		7.897	0.15300
0.3	1	5.898	0.36300
0.4		6.782	1.43200
0.2		3.658	0.09011
0.3	2	1.789	0.16370
0.4		7.517	0.37340
0.2		2.237	0.08431
0.3	3	6.767	0.14770
0.4		2.842	0.12230

889

890 Table 8

891 Measures of fit of multiple regression analysis at different experimental conditions for α and R_p:
892 values of R^2.

MRA	α	R_p
	R^2	R^2
1	0.210	0.958
2	0.167	**0.965**
3	0.765	0.874
4	**0.884**	0.874

893

894 Table 9

895 Fitted transition time between stages for Yee's model.

ΔP	v	Stage 1	Stage 2
(MPa)	(m/s)	t_1 (s)	t_2 (s)
0.1	1	4076.00	12400.00
0.2		742.41	2991.00
0.3		570.21	3545.00
0.4		440.74	4739.00
0.1	2	4812.00	8689.00
0.2		2291.00	8151.00
0.3		1389.00	5640.00
0.4		558.76	8212.00
0.1	3	2092.00	13000.00
0.2		5138.00	9946.00
0.3		430.54	6669.00
0.4		794.04	15980.00

896

Figure
Click here to download Figure: renamed_58b2f.docx

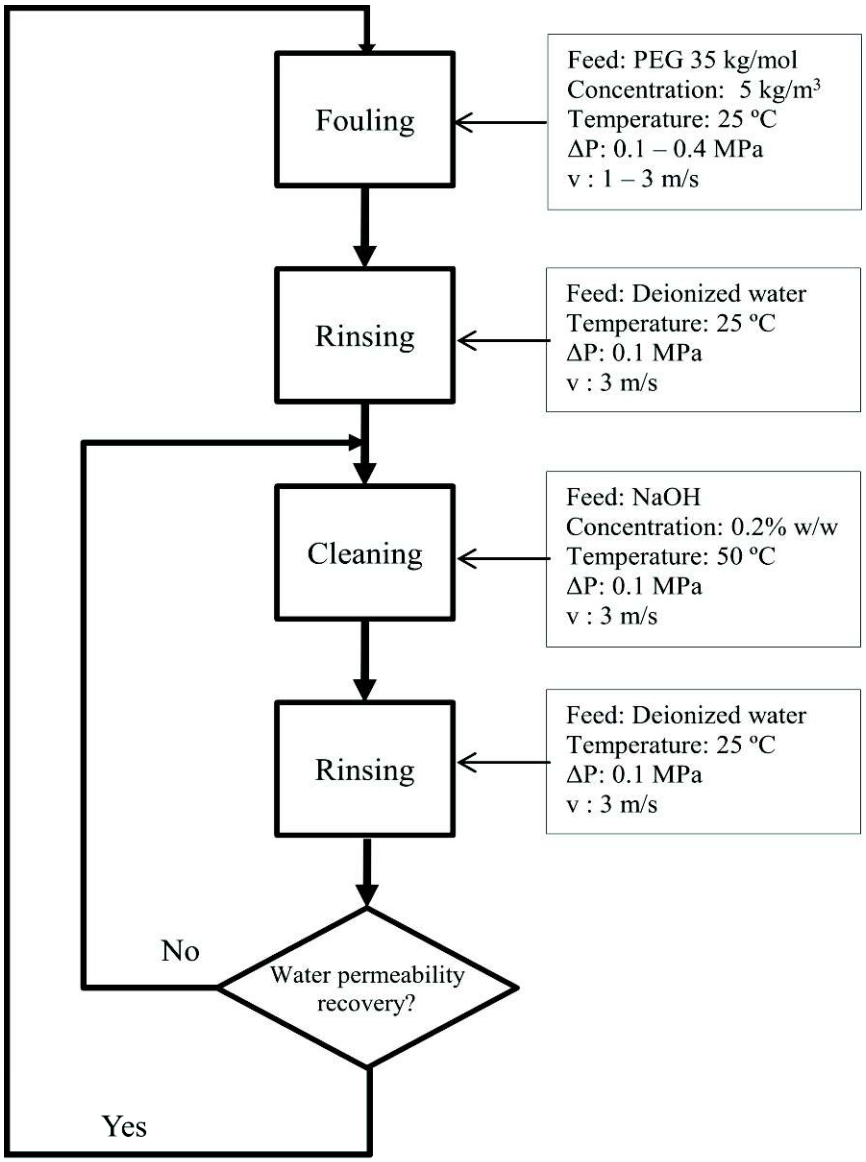

Fig. 1 Experimental procedure

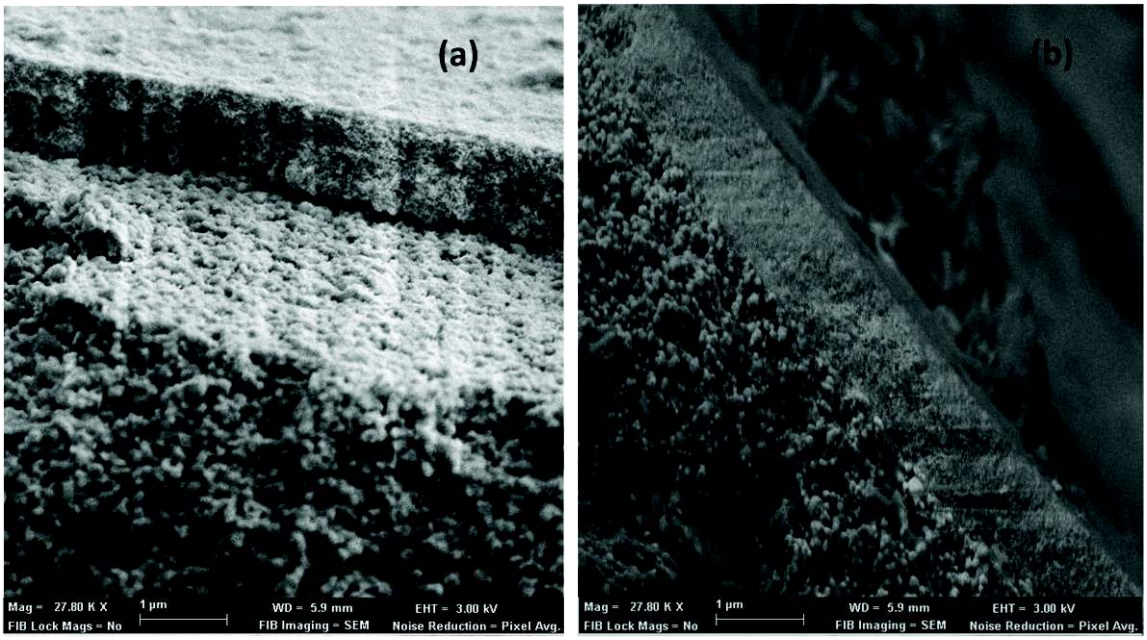

Fig. 2 Cross-section of new (a) and fouled (b) membranes at X27800 of magnification

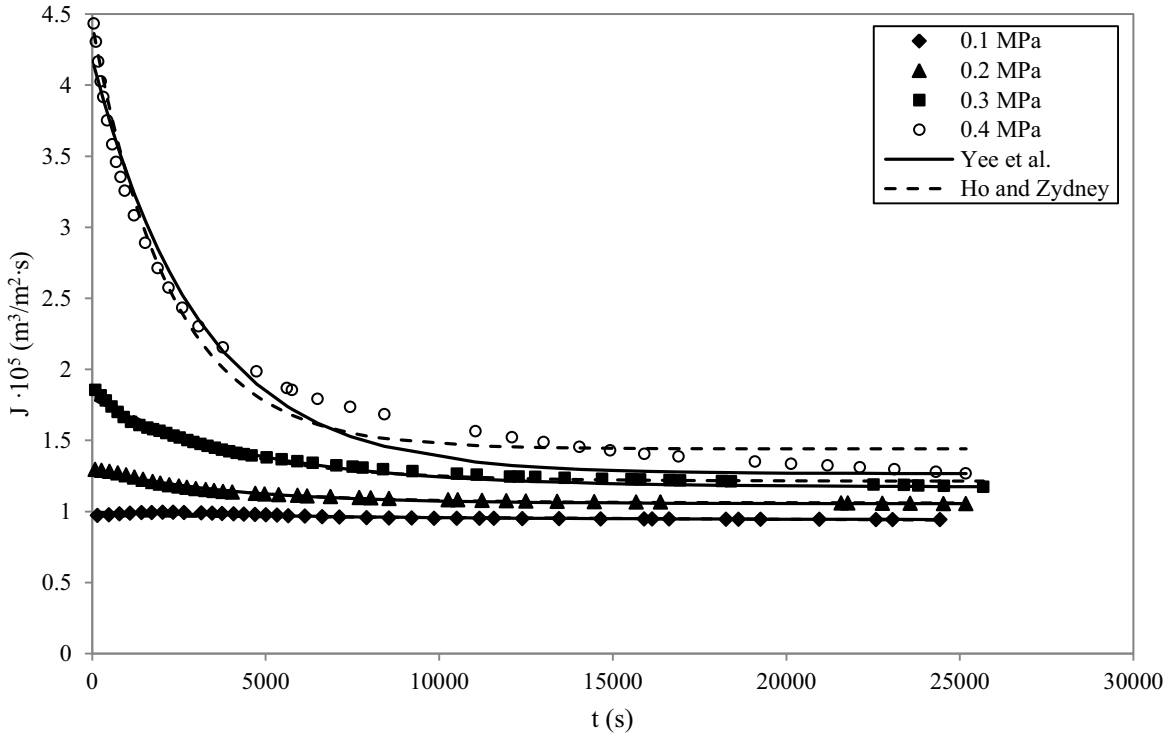

Fig. 3 Permeate flux predictions for Ho and Zydney's model (dotted line) and Yee's model for one stage (solid line) at different transmembrane pressures for a crossflow velocity of 1 m/s, (symbols: experimental data)

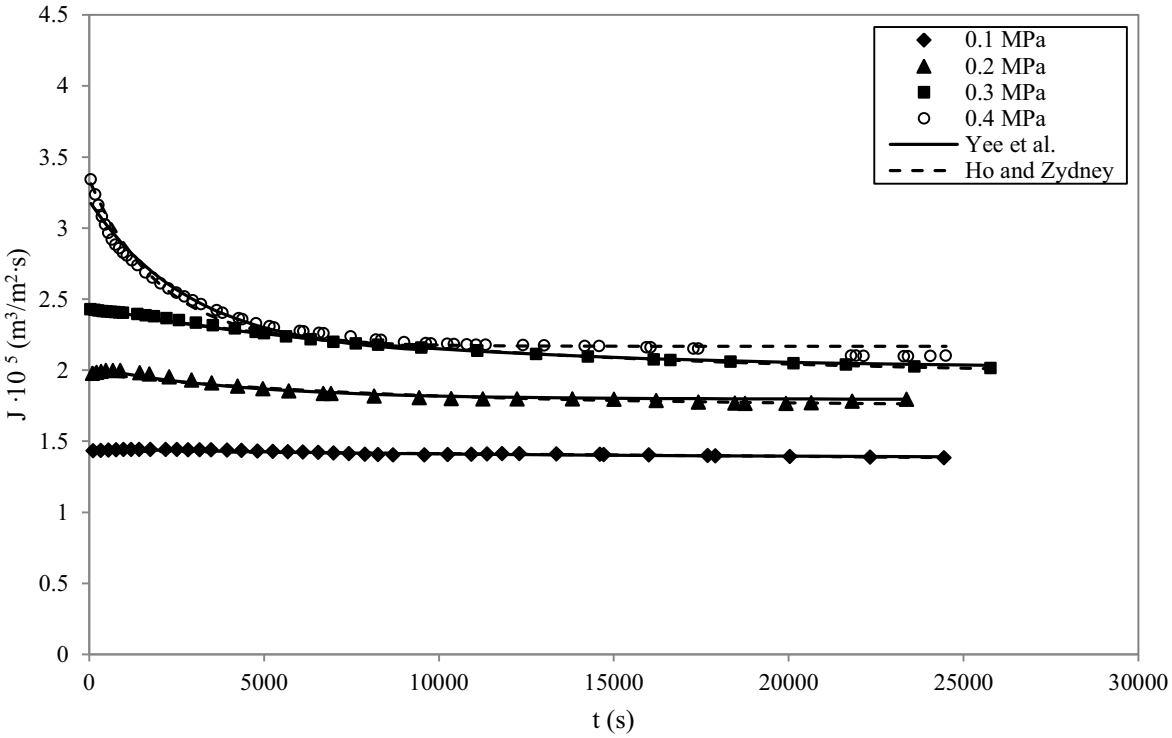

Fig. 4 Permeate flux predictions for Ho and Zydney's model (dotted line) and Yee's model for one stage (solid line) at different transmembrane pressures for a crossflow velocity of 2 m/s, (symbols: experimental data)

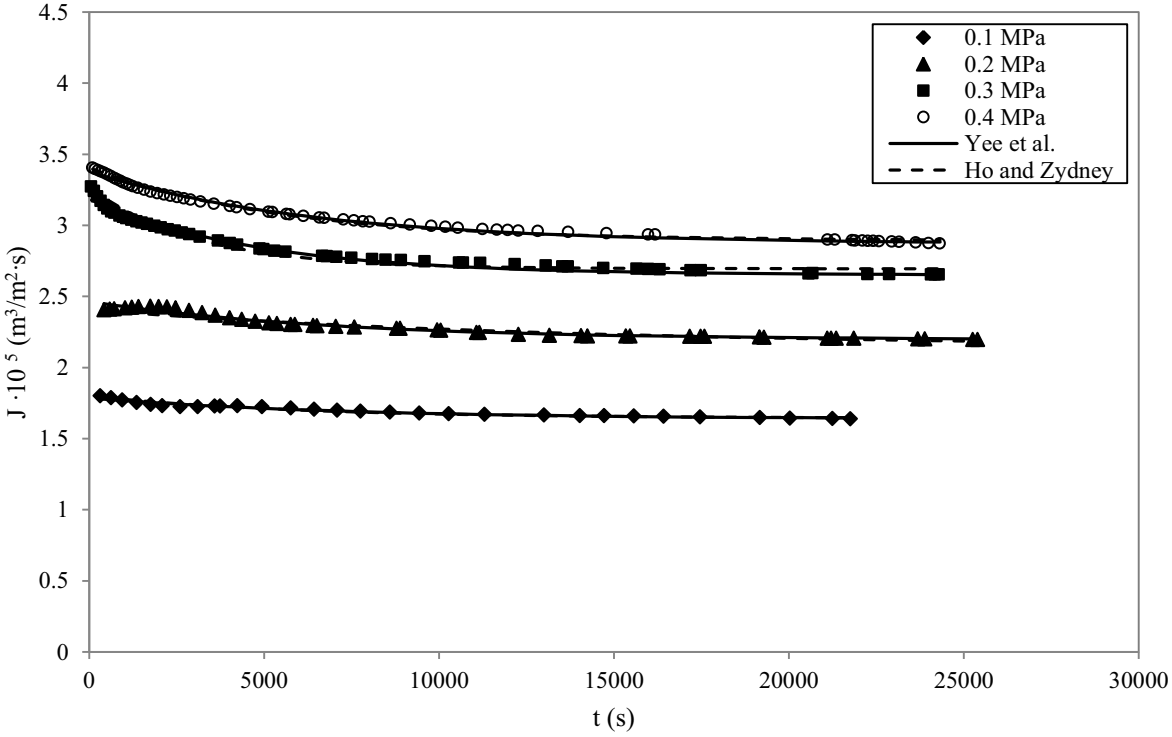

Fig. 5 Permeate flux predictions for Ho and Zydney's model (dotted line) and Yee's model for one stage (solid line) at different transmembrane pressures for a crossflow velocity of 3 m/s, (symbols: experimental data)

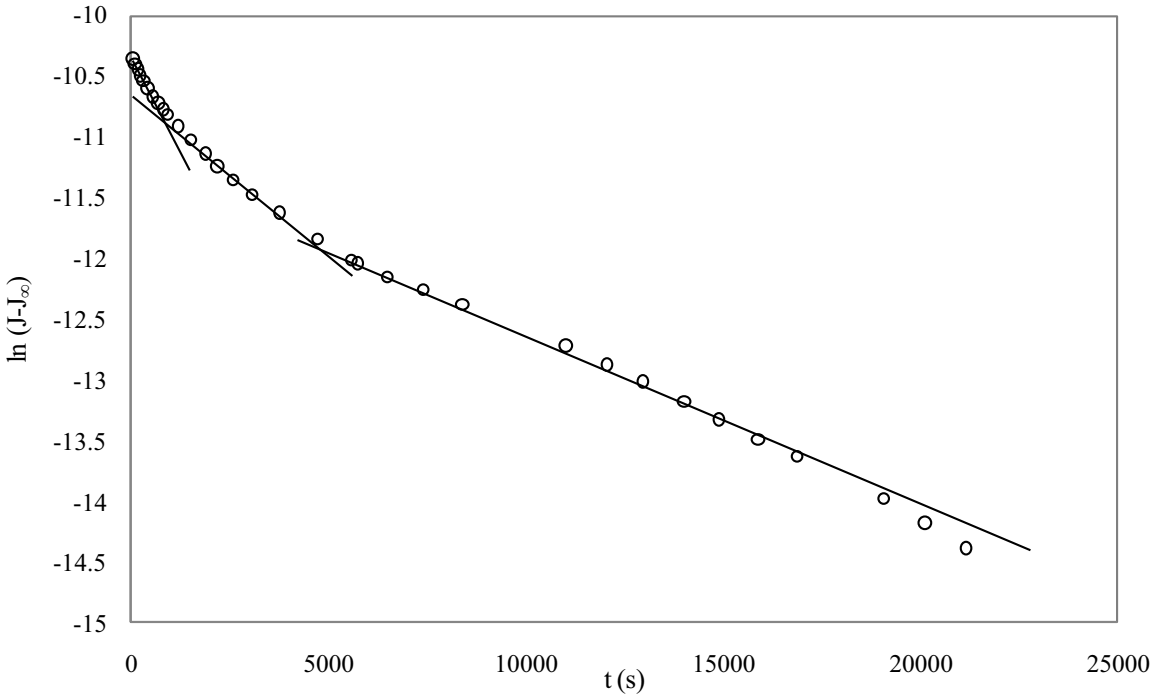

Fig. 6 Evolution of ln(J-J_∞) with time for a transmembrane pressure of 0.4 MPa and a crossflow velocity of 1 m/s, (lines: estimated results; symbols: experimental data)